Integrated Structural and Optical Modeling of the Orbiting Stellar Interferometer

S. Shaklan, J. Yu, and H.C. Briggs
Jet Propulsion Laboratory
California Institute of Technology
4800 Oak Grove Drive
M/S T1701
Pasadena, CA 91109

ABSTRACT

The Integrated Modeling of Optical Systems (IMOS) Integration Workbench at JPL has been used to model the effects of structural perturbations on the optics in the proposed Orbiting Stellar Interferometer (OS1). OS1 consists of 3 pairs of interferometers and delay lines attached to a 7.5 meter truss. They are interferometrically monitored from a separate boom by a laser metrology system. The spatially distributed nature of the science instrument calls for a high level of integration between the optics and support structure. Because OSI is designed to achieve micro-arcsecond astrometry, many of its alignment, stability, and knowledge tolerances are in the sub-micron regime. The spacecraft will be subject to vibrations caused by reaction wheels and on-board equipment, as well as thermal strain due to solar and terrestrial heating. These perturbations affect optical parameters such as optical path differences and beam co parallelism which are critical to instrument performance. IMOS provides an environment that allows one to design and perturb the structure, attach optics to structural or 110]1-Structural nodes, trace rays, and analyze the impact of mechanical perturbations on optical performance. This toed makes it simple to change the structure and immediately see performance enhancement/degradation. We have employed IMOS to analyze the effect of reaction wheel disturbances on the optical path difference in both the science and metrology interferometers.

1 INTRODUCTION

The Orbiting Stellar Interferometer (OSI) has been proposed as a space-based instrument that can obtain micro-arcsecond (5×10^{-12} radian) astrometric precision [1]. This instrument will accomplish a large number of science objectives including improved knowledge of distance to Cephied variables, finding extra-solar planets, and the dynamics of globular clusters. Additionally, the instrument is capable of forming images with 3 times the resolution of the Hubble Space Telescope.

OS1 consists of 6 siderostats that form 3 pairs of optical interferometers, plus a seventh siderostat that acts as a spare. The spacecraft is composed of two booms: the siderostat boom contains all the long-baseline optics ant] all flight systems; the metrology boom supports an external metrology system that monitors relative motions of the siderostats. Figure 1 shows a diagram of the main optical components configured in the spacecraft.

OS1 measures the angular distance between stars by adjusting the positions of delay lines until white light fringes are observed in each of3 baselines. The position of the delay lines relative to the other optics is monitored by internal metrology laser beams (not shown in Figure 1) that follow the optical path of the starlight through the interferometers before retroreflecting from corner cubes mounted on the siderostats. External metrology beams originating from the metrology triangle monitor the positions in 3-space of the siderostats from the same corner cubes shared by the internal metrology beams. The external metrology beams determine the relative orientation and length of the baselines, while the internal metrology beams monitor optical path differences between the two arms of the interferometer.

Two siderostat pairs observe bright reference sources while the third pair observes the science object. The two reference siderostats provide high precision attitude knowledge for rotation about the Y and Z axes, while a star tracker indicates the less critical roll about the X axis (Fig. 1). Attitude knowledge determined from the reference baselines, combined with the internal and external metrology signals, allows an absolute determination of the angle

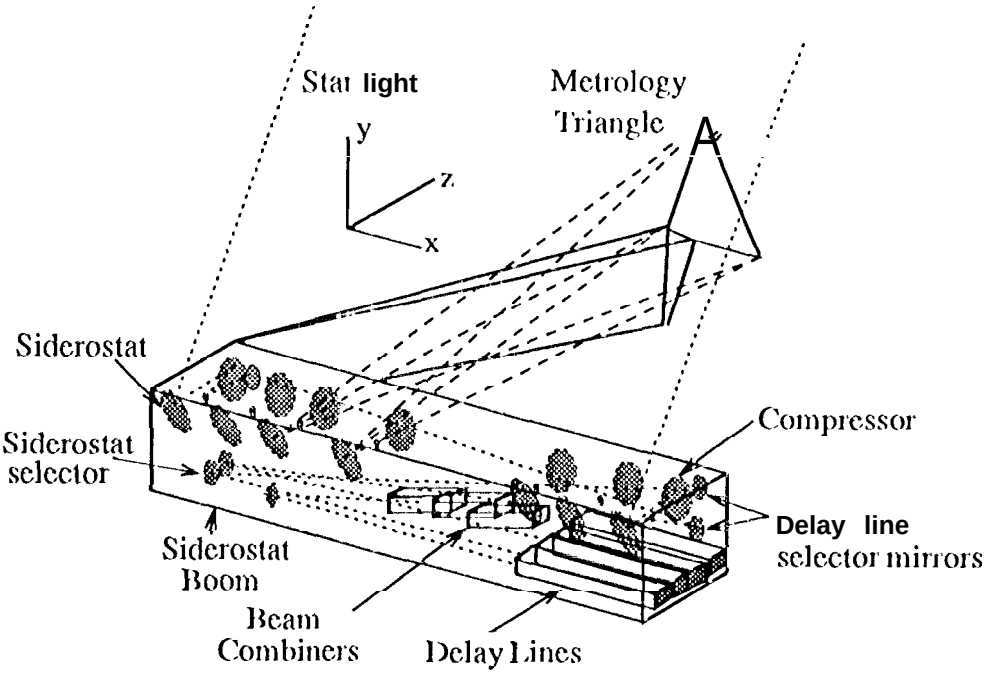

Figure 1: The Orbiting Stellar Interferometer. This diagram shows most of the key optical components for two siderostat/beam-combiner trains.

between the two reference stars and the science object. For astrometry, this fixes the position of a star along a line; the other dimension is determined by rotating the spacecraft and repeating the measurement.

To achieve micro-arcsecond precision, both starlight and internal and external metrology optical paths must be measured at sub-nanometer levels. This requires an understanding of how the mechanical disturbances propagate through the structure and perturb the optical beams at the beam combiners. To accomplish this we use a new tool, the Integrated Modeling of Optical Systems (IMOS) workbench [2,3,4]. IMOS is a set of structural, optical, and thermal modeling tools that all function in a single Pro-Matlab [5] based environment.

The IMOS structural model is based on beams, rods, plates and masses that are all connected to a set of grid-points. Functions exist for assembling the mass and stiffness matricies, converting a dynamics or modal model to state-space form, and performing a Guyan reduction of the model. The optics module is based on the Controlled Optics Modeling Package (COMP) [6]. COMP is a set of stand-alone and subroutine-based computer tools for performing large ray traces, near and far-field diffraction computations, and linear differential ray-traces. As described in section 3, the sensitivity matrix derived from the differential ray-traces provides a direct link of the optics model to the structure. The thermal module in IMOS is based on the Thermal Radiation Analysis System (TRASYS) and the Systems Integrated Numerical Differencing Analyzer (SINDA) programs. In it's current implementation, IMOS is used to compute input files for SINDA and TRASYS. These programs are executed outside the Pro-Matlab environment, and produce thermal force inputs that are used by IMOS to compute thermal loads. In future versions, the thermal module will be more highly integrated to the optics and mechanics portions of the code.

2 OSI STRUCTURE AND OPTICS

2.1 Structure

The IMOS structural model of OSI consists of 139 aluminum beams, each about 1 m long, and 35 plates, each about 1 m^2, connected as shown in Figure 2. Additionally, there are 39 point masses distributed along the structure, each

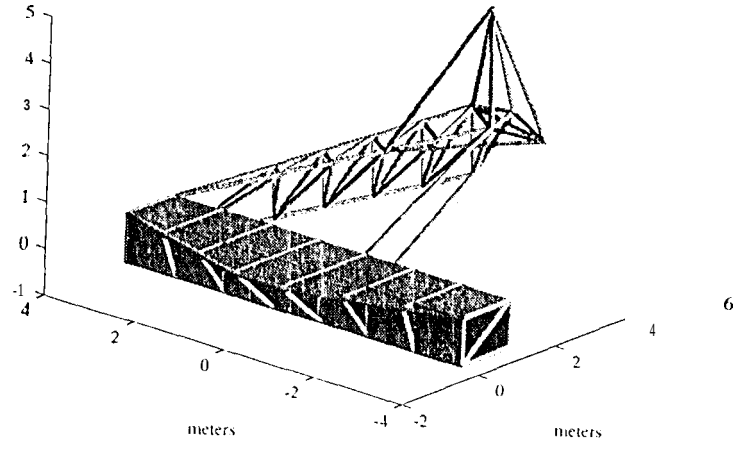

Figure 2: The IMOS structural model of 0S1. Plates covering the siderostat boom add stiffness and distribute thermal loads. Holes in the plates that allow starlight to enter the interferometer are not shown.

connected by a tripod to the three closest grid points. These masses represent the optics and key system components such as power systems, reaction wheels, etc. Some components, such as the siderostat, primary, secondary, and fast-steering mirror of a siderostat bay, arc lumped into one mass. The total mass of the spacecraft is 1658 Kg, of which 1475 Kg is non-structural.

The structure is divided into the siderostat boom and metrology boot-n. After launch, the metrology boom and metrology triangle arc deployed into the position shown in Figures 1 and **2. In** the IMOS model, hinges arc assumed to be rigid after deployment. in addition, the support, beams between the siderostat boom and the end of the metrology boom are also assumed to be rigid after deployment.

All grid points associated with a beam element (having axial, torsional, and 2 transverse bending stiffnesses) have 6 degrees of freedom. Grid points associated with masses (which arc points and therefore have no rotational inertia terms) have only translational degrees of freedom. In total, the model has 441 degrees of freedom. We note that the computational time for constructing the mass and stiffness matricies and determining the structural modes is about 20 minutes on a SunSPARC 2 workstation.

2 , 2 Optics

The dotted lines in Figure 1 show the optical path followed by starlight. in each of 2 optical trains, the light first reflects off of a siderostat, then is compressed from a 33 cIn beam to 2.5 cm. After passing through the center of the compressor primary, a fast-steering mirror directs the light to a bank of mirrors that select one of 8 delay lines. These mirrors direct the light across the siderostat boom to a second set of articulating mirrors that arc pointed between a siderostat and beam combiner. This allows any siderostat to usc any delay line. After retroreflecting in the delay line, which is composed of a parabola and flat secondary, the light then enters the beam combiners where it is interfered at a bcaln-splitter with light from another siderostat.

A full optical prescription was designed for two optical trains following light from siderostats 1 and 7 (at opposite ends of the siderostat boom, as seen in Figure 1). Along with the usual optical prescription data, the COMP model includes a rotation/translation point for each element. In our case, we take this point to be tied to the closest

structural grid point, so that motions of the optical elements are related by an imaginary lever arm tied to their respective grid points. When the structure is perturbed, motions of the optics are tied to these grid points via the optical sensitivity matrix.

in the COMP environment, a differential ray trace is performed. This ray trace determines the sensitivity of a ray to motion of the elements. The resulting matrix, called C_{opt} has 7R x 6N elements, where N is the number of optical elements in the beam train, and R is the number of rays traced. Since we are only interested in OPD fluctuations and beam deviations, just the chief ray is used in our simulations. For the current 0S1 model, N= 10. The 7 rows are for ray direction perturbation (3 rows), ray transverse aberration (3 rows), and ray optical path difference (1 row), Each element can be perturbed in 6 degrees of freedom, thus the matrix is 7 x 6N.

A separate sensitivity matrix is computed for each optical train. The matricies are then exported from COMP to the IMOS environment.

3 OPTICAL/STRUCTURAL INTEGRATION

IMOS assembles the structure into a mass matrix M and stiffness matrix K. The Pro-Matlab function "eig" is then used to find the eigenvectors and eigenvalues of M-1 K. The eigenvectors are mode shapes and eigenvalues are squared modal frequencies. Modal vectors are then normalized to unity modal mass. With this normalization, the equation of motion for the structure can be written

$$\dot{\vec{x}} = \begin{bmatrix} 0_{MM} & I_{MM} \\ \omega^2_{MM} & -2\zeta\omega_{MM} \end{bmatrix} \vec{x} + \begin{bmatrix} 0_{Mi} \\ (\Phi_{Mi})^t \end{bmatrix} \vec{u} \tag{1}$$

where

$$\vec{x} = \begin{bmatrix} \vec{\eta} \\ \dot{\vec{\eta}} \end{bmatrix}$$

and $\vec{\eta}$ is the modal state vector, representing the amplitude of each of the M modes. Subscripts represent the size of the sub-matricies. O is a matrix of zeros, and I is the identity matrix. w is a diagonal matrix of modal frequencies, while ζ is the diagonal modal damping matrix. $\vec{u}$ is the force input vector; it's i elements are the degrees of freedom where forces are to be applied to the structure. Φ is an array whose M columns are each a mode shape and whose i rows are mode displacements for the degrees of freedom specified by $\vec{u}$. Φ is a subset of the full modeshape matrix. Note that Φ^t, the transpose of Φ is used here.

The equations of motion are combined with the measurement equation

$$\vec{y} = [\Phi_{cM} \;\; 0_{cM}]\,\vec{x} \tag{2}$$

where Φ is again a subset of the full modeshape matrix. It's c rows represent the degrees of freedom that are to be analyzed. Each element of $\vec{y}$ is the motion of a specific degree of freedom (1)01).

Equations (1) and (2) are combined in the general first-order state-space form given by

$$\dot{\vec{x}} = A\vec{x} + B\vec{u} \tag{3}$$

$$\vec{y} = C\vec{x} \tag{4}$$

where the definitions of A, B, and C can be inferred from the collations. Once in state-space form, the system can then be exercised by standard MATLAB functions "lsim" for linear time simulations and "bode" for transfer function analysis.

Optics are integrated into this system by modifying the measurement equation (eq. 4). The C matrix converts modal amplitudes to DOF motions, while the optical sensitivity matrix, C_{opt}, converts DOF motions to optical ray perturbations. By selecting in C the same DOF subset specified in C_{opt}, a new measurement equation is formed where the outputs $\vec{y}$ [are the optics] perturbations desired in the analysis:

$$\vec{y} = C_{opt}C\vec{x} = C_{net}\vec{x} \tag{5}$$

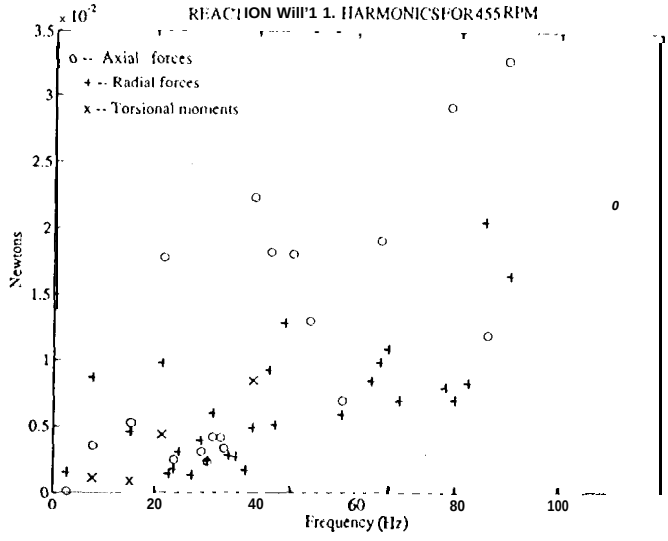

Figure 3: HST reaction wheel harmonics for a wheel speed of 455 rpm. For the reaction wheel implemented in our OS1 study, torsional moments are applied about the z-axis, axial forces are along the z-axis, and radial forces are in the x-y plane.

Note that $\vec{y}$ can still include non-optical terms as well. Rows can always be added to the C_{net} matrix that convert $\vec{x}$ to a desired measurement. In the present case, angular motions of the metrology boom relative to the end of the siderostat boom were also included in the measurement equation.

As noted above, C_{opt} is computed for the optical train of each interferometer arm. Since we are interested only in the optical path differences and relative angular deviations between the beams that reach the beam combiner, we subtract the two C_{opt} matricies from one another so that the measurement equation is actually

$$\vec{y} = (C_{opt,1} - C_{opt,2})C\vec{x} = C_{net}\vec{x} \ . \tag{6}$$

4 REACTION WHEEL MODEL

OS1 currently uses the Honeywell HR195 reaction wheel as part of its attitude control system. This is the same wheel that is being used in the Hubble Space Telescope. This wheel has a maximum angular momentum of 264 Nms, output torque of 0.7 Nm, and maximum speed of 3000 rpm. OSI has a slew requirement of 114° in 20 minutes. (This is based upon orbital parameters, sun/earth view restrictions, and minimum integration time/orbit.) For a bang-bang controller employing the HST reaction wheel, the reaction wheel achieves the required slew rate by spinning Up to 455 rpm in 10 minutes.

The HST reaction wheels have undergone thorough vibrational tests [7]. They exhibit radial, axial, and torsional forces, each with several harmonics of the rotational speed. Figure 3 shows a plot of these forces for a wheel speed of 455 rpm. The forces for a given harmonic all increase quadratically with wheel speed.

We have modeled a single reaction wheel that is attached to the structural grid point that is closest to the spacecraft's center of mass. The reaction wheel is assumed to be located exactly at that grid point, and is attached either rigidly or via a clamping mechanism. The wheel spins shout the z-axis, so that the axial forces are applied along, z, the torsional moments arc about the z-axis, and radial forces arc in the. x-y plane.

The isolator is based on a design by Davis [8]. It is a second order damper with break frequency at 4 Hz.

SHARLANS

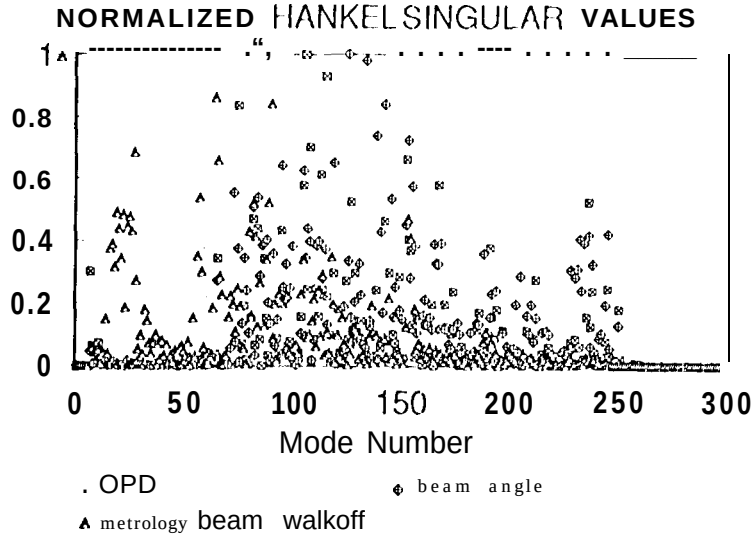

Figure 4: Normalized Hankel singular values for three different cost functions. Modes beyond 300 arc would indistinguishable from zero on this plot.

Further det ails arc given by Melody [9]. The implementation of the isolator assumes that there is no dynamic interaction Let ween th c isolator and the structure. This may not be a good assumption since the lowest modes of the structure resonate at 5-10112.

5 MODELING

5.1 Hankel Singular Values

The **free-free model has 441** degrees of freedom and therefore generates 441 modes. It is desirable to reduce the actual number of modes used in the modeling by eliminating those modes that contribute little to the metrics of interest. To accomplish this, we evaluate the Hankel singular values (HSV) for each mode and for each desired output. Hankel singular values are essentially a product of a mode's output contribution and controlability, weighted by the mode's eigenvalue (frequency^2). Output contributions arc computed by multiplying the optical sensitivity matrix (or other suitable matrix, depending on the desired output) by the modes of the system. Controlability is computed by multiplying the transpose of the mode matrix by an array with degrees of freedom set according to the force inputs. in our case, these are the degrees of freedom associated with the grid point where the reaction wheel is attached. A mathematical description of this process is given by Melody [9].

Figure 4 shows the normalized HSVs for all 441 modes for three cases: OPD between the two siderostat trains, relative angular deviations between the beams, and angular changes of the tip of the metrology boom with respect to the tip of the siderostat boom. The OPD and angular deviation symbols show that low order modes contribute little to siderostat errors. This is because the lower modes arc mainly flexures of the metrology troom. The triangles in Fig. 4 verify this. These plots indicate which modes should be targeted for damping using passive or active struts.

We have parcel down the number of modes from 441 to 158 by keeping only those modes that have. HSVs >0.1 in any of the three output functions. This results in a mode distribution that covers the frequency range from 5 Hz (the first non-rigid body mode) to 639 Hz (mode 250), plus the 6 rigid body modes.

5.2 Frequency Domain Modeling,

Our modeling takes place in the frequency domain. The transfer function of the system is computed for each of the 4 input, forces using Pro-Matlab function "Bode." The 4 forces are radial reaction wheel harmonics in x and y (2), axial harmonics in Z (l), and torsional moments around the z axis (1). Each call to Bode results in 7 transfer functions: 3 optical beam angular deviations, one OPD, and three angular deviations of the tip of the metrology triangle with respect to the end of the siderostat boom. Transfer functions arc evaluated in 1 Hz steps between 1 Hz and 1 kHz.

WC then choose a wheel speed and determine its harmonics. The Bode plots arc interpolated at the reaction wheel harmonics, and the interpolated Bode amplitudes are multiplied by the reaction wheel forces. The results arc then added in quadrature for each of the 7 outputs.

Outputs 1-3 are combined in quadrature to yield the r.m.s. angular deviations between the beams in the beam combiner. Outputs 5-'7 are similarly combined to yield r.in.s. angular motion of the metrology boom. The angular deviations are multiplied by the nominal vector joining the tip of the metrology boom the the end of the siderostat boom. Output 4 is the r.in.s. OPD between the siderostat trains.

6 RESULTS

6.1 Non-isolated Reaction Wheel

Figure 5 (left column) shows results for the three outputs when the reaction wheel is directly coupled to the structure without any isolation. Nominal wheel speeds of ≈ 200 rpm can be expected. (The bias is used to prevent the wheel from ever reversing direction when gravity gradients become large.) Figure 5b shows the visibility loss due to angular deviations. The visibility loss is given approximately by

$$V = - \left|\mathrm{sinc}(2 * \pi * \sigma_\theta * d/\lambda)\right|, \tag{7}$$

where σ_θ is the r.in.s. angular deviation, d is beam diameter, and λ is the wavelength (taken as 0.55 pin). Figures 5 (top and middle) show that at wheel speeds greater than 600 rpm, the undamped reaction wheel induces optical errors that exceed allowable tolerances.

6 . 2 Isolated Reaction Wheel

Figure 5 (right column) shows the results when the isolator described in section 4 is used to couple the reaction wheel to the structure. For OPD and beam angular fluctuations, the isolator has little effect for wheel speeds below 400 rpm. "his is because low order (low frequency) modes do not affect these terms; only higher wheel harmonics at these low speeds induce optical errors. At higher wheel speeds, the isolator reduces the maximum OPD error from 75 rim at to about 3 nm. Visibility loss due to rms angular deviations is rendered essentially negligible. Metrology beam walkoff, which is sensitive to low order modes (flexures of the metrology boom), is greatly improved above 100 rpm.

7 CONCLUSION

Unlike previous models of an orbiting interferometer [10], in which the optical and structural models were contained in separate environments, the IMOS model provides a means of directly analyzing optical performance in the presence of structural perturbations. The perturbations may be either mechanical or thermal in nature.

lhd-users of IMOS must have some familiarity with finite element modeling. Armed with the basics of linear algebra and a few fundamentals of mechanical structures, IMOS allows the engineer to understand optical/mechanical/thermal interactions without the constraints imposed by stand-alone solutions such as NASTRAN, SINDA/TRASYS, CODE V, or COMP. More importantly, with the IMOS workbench, the subsystems can be

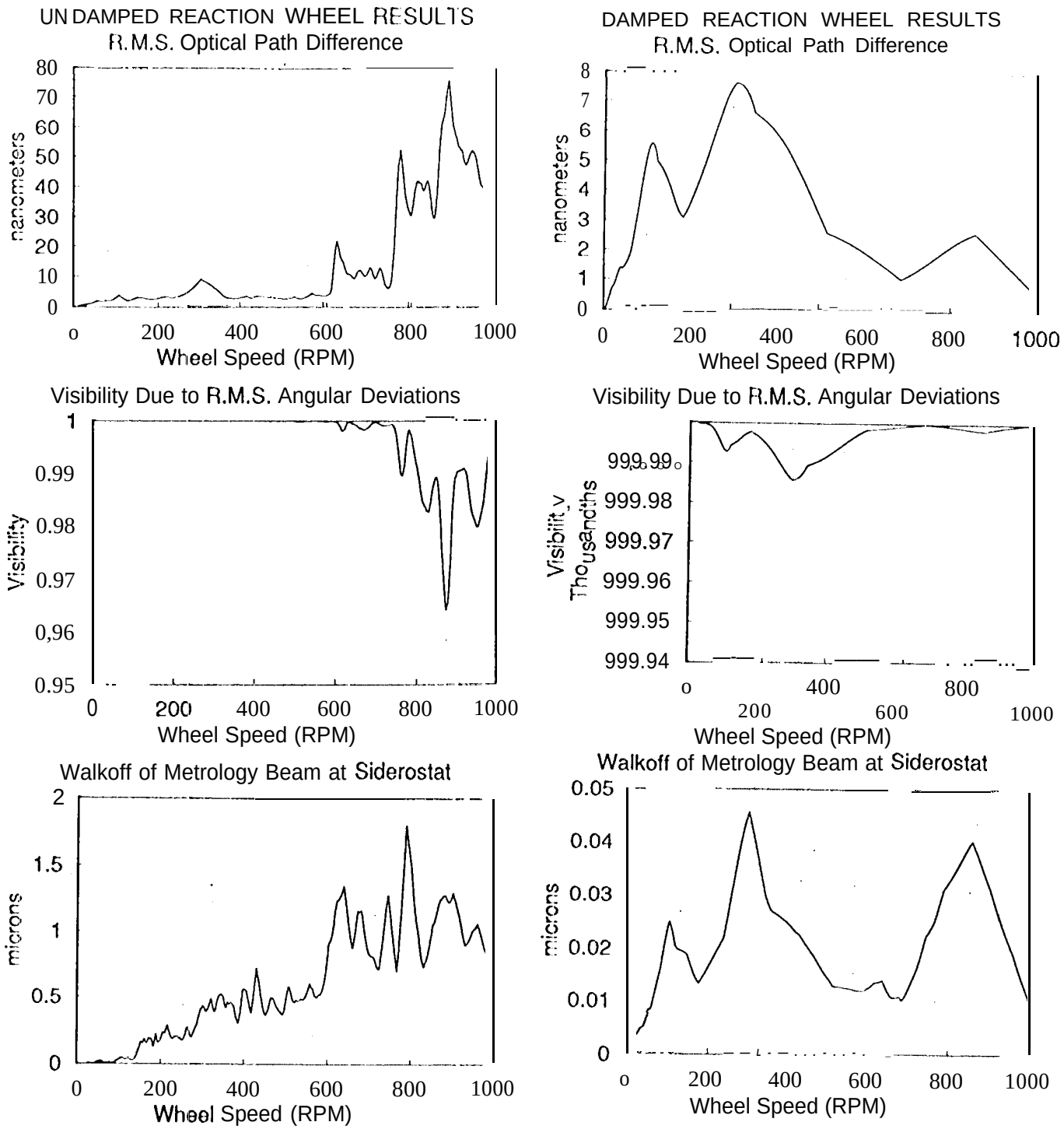

Figure 5: **Reaction wheel vibration results. Left** column is for a non-isolated reaction wheel. Right column **uses** the isolator **described** in section **4**. Top: **RMS** OPD between optical trains from **siderostats** 1 and 7. Middle: **RMS** visibility loss clue to relative angular **deviations** between the beams as **they** are combined on the detector. **Bottom: Walkoff** of a **metrology** laser beam **on** a **corner cube** located on **siderostat** 7.

redesigned or modified allowing immediate understanding of the impact on other subsystems as well as overall system performance.

The results presented in this paper represent only the beginnings of our OSI study. We are currently implementing the thermal module. Earth/Sun heating in a realistic orbital scenario will cause the structure to deform. In the thermal problem, which is slow but potentially of large amplitude, we are concerned that deformation may cause large misalignments that exceed the limitations of guiding optics.

The structural work is also progressing. We have identified which modes are most costly in terms of OPD and visibility loss. This allows us to target particular parts of the structure for passive or active dampers. We are also inverting the reaction wheel problem; given optical tolerances, we can set tolerances on the allowable structural perturbations. This could potentially lead to a cost savings if less expensive (but noisier) reaction wheels are found to be capable of meeting the slew requirements.

8 ACKNOWLEDGEMENTS

We are pleased to acknowledge the assistance of J. Melody, who provided the reaction wheel and isolator models, as well as numerous other useful subroutines. We would like to thank J. Melody, L. Needles, W. Ledeboer, M. Millman, R. Norton, and P. Maiocco for numerous technical discussions. L. Tenn created the first structural models of OSI. The Jet Propulsion Laboratory is operated by the California Institute of Technology, under contract with the National Aeronautics and Space Administration.

References

[1] M.M. Colavita, M. Shao, and M.D. Rayman, "OSI: Orbiting Stellar Interferometer for Astrometry and Imaging," *Appl. Opt.*, **in press.**

[2] H.C. Briggs, L. Needels, and B.M. Levine, "Integrated Modeling of Advanced Optical Systems," Proc. of the 5th NASA/DOD Control/Structure Interaction Technology Conference (Lake Tahoe, March 1992).

[3] H.C. Briggs, "An Integrated Structure/Optics/Control Modeling and Analysis Software Breadboard," Proc. of the 4th NASA/DOD Control/Structure interaction Technology Conference (Orlando, Nov. 1990).

[4] H.C. Briggs and L. Needels, "Integrated Multidisciplinary Analysis of Segmented Reflector Telescopes," Proc. SPIE Vol 1696 (Orlando, April 1992).

[5] Pro-Matlab is available from The MathWorks, Inc., Natick, Mass.

[6] D. Redding and W. Breckinridge, "Optical Modeling for Dynamics and Control Analysis," J.G.C.D, Vol 14, p. **1021,** 1991.

[7] M.D. Hasha, "Reaction Wheel Mechanical Noise Variations," Space Telescope Program Engineering Memorandum SSS 218, Lockheed Missile and Space Center (30 June 1986).

[8] D. Cunningham, P. Davis, and F. Schmidt, "A Multi-axis isolation System for the French Earth Observation Satellite's Magnetic Bearing Reaction Wheel," Proc. ADPA/AIAA/ASME/SPIE Conf. on Active Materials and Adaptive Strut.turcs (Alexadria, Va, Nov. 1991).

[9] J. Melody and H.C. Briggs, "Analysis of Structural and Optical Interactions of the Precision Optical Interferometer in Space (POINTS)," Proc. SPIE Conference on Spaceborne Interferometry Vol. 1947 (Orlando, April, 1993).

[10] R. Laskin, ed., "Focus Mission Interferometer 'Business-As-Usual' Design Document," Jet Propulsion Laboratory Document D-6916 (Pasadena, Ca, Oct. 1989).